Nanoscale Advances

ROYAL SOCIETY OF CHEMISTRY

PAPER

View Article Online
View Journal | View Issue

Cite this: *Nanoscale Adv.*, 2024, **6**, 5398

A Pd-containing ionic liquid modified magnetic graphene oxide nanocomposite (Fe_3O_4/GO–IL–Pd) as a powerful catalyst for the reduction of nitrobenzenes

Farkhondeh Dadvar and Dawood Elhamifar *

A novel palladium-containing ionic liquid-modified magnetic graphene oxide nanocomposite (Fe_3O_4/GO–IL–Pd) is synthesized and its catalytic performance is studied in the reduction of nitrobenzenes. The Fe_3O_4/GO–IL–Pd nanocomposite was characterized by using FT-IR, PXRD, SEM, EDS, VSM, and TG analyses. These analyses showed good magnetic properties and high stability of the designed composite. Different derivatives of nitrobenzenes were applied as substrates, giving corresponding anilines in high to excellent yields (89–96%) at short reaction times (10–15 minutes). Also, the stability, reproducibility, and reusability of the Fe_3O_4/GO–IL–Pd nanocomposite were investigated under applied conditions. A leaching experiment was also performed to study the nature of the Fe_3O_4/GO–IL–Pd catalyst under the conditions used.

Received 8th June 2024
Accepted 18th August 2024

DOI: 10.1039/d4na00475b

rsc.li/nanoscale-advances

1. Introduction

As a type of nitrogen-containing organic compound, aniline derivatives have several applications in chemical industries such as dyes, antioxidants, medicines, and agricultural chemicals.[1–4] In addition, anilines are building blocks for the preparation of rubber products, textiles, electronic instruments, photography, coatings, pharmaceuticals, consumer goods, *etc.*[5] An efficient method for the preparation of aniline derivatives is the reduction of nitrobenzenes by using molecular hydrogen,[6] hydrazine hydrate,[7] $NaBH_4$,[8] sodium hydrosulfite,[9] and sodium formate.[10] Considering the slow or impossible conversion of nitrobenzenes to aniline derivatives, the reduction of these compounds is performed in the presence of homogeneous metal catalysts.[11,12] Due to the limitations of homogeneous catalysts such as non-recoverability, difficulty in separation of products, and high cost of their extraction and processing, researchers are looking for cheaper and more accessible catalysts or the maximum use of the catalytic capacity of these valuable metals. Stabilization of homogeneous catalysts on solid supports is considered one of the suitable methods to solve these limitations.[13–15] Some recent reports about immobilization of metal catalysts on solid supports are Cu-MOF,[16] Fe_3O_4@Fritillaria/Pd,[17] Ni/carbon,[18] and AuNP@PPh_2–PIILP.[19]

Among different catalytic supports, carbon nanostructures are very attractive owing to their low price, high strength, and good stability.[19–21] In addition, due to their high surface area, low weight, great flexibility, and outstanding electrical conductivity, carbon materials such as graphite, graphene oxide (GO), and fullerenes have many applications in medicine, agriculture, drug delivery, and chemistry.[19,22,23] Among these, graphene oxide, obtained from the oxidation of graphene, has monolayered sp^2 hybridization with unique chemical and physical properties. The carboxyl and hydroxyl functions of GO make it a suitable support for the stabilization of organic and inorganic compounds.[24–31] For example, various chemicals such as UiO-66–$(COOH)_2$,[27] chitosan, graphite carbon nitride,[32] and gelatin are well immobilized on GO.[33] However, separation of GO is difficult due to the presence of amphoteric groups in its structure. Therefore, coating GO on magnetic nanoparticles (MNPs), to form magnetic-GO composites, solves this problem and improves its performance to expand catalytic applications.[34,35] Some advantages of magnetic-GO nanocomposites are their easy synthesis, high surface area, and easy separation from the reaction medium.[36,37] Different magnetic nanoparticles such as Co_3O_4, NiO_2, Fe_2O_3, and Fe_3O_4 have been used to magnetize GO-containing composites. Among these, Fe_3O_4 is the best one due to its more stability, less toxicity, and high biodegradability and biocompatibility.[38,39] According to the literature, various composites containing GO and magnetic nanoparticles such as GO/$CoFe_2O_4$,[40] AMGO–Glu@Fe_3O_4,[41] F_3O_4@GO/PS,[42] a-Fe_2O_3–rGO,[43] graphene/Fe_3O_4/NiO,[44] and rGO/NiO,[45] have been prepared.

On the other hand, imidazolium-based ionic liquids (ILs) have been proposed as excellent stabilizers for transition metal (TM) nanocatalysts to prevent their accumulation in catalytic transformations and increase their stability.[46,47] Properties such

Department of Chemistry, Yasouj University, Yasouj, 75918-74831, Iran. E-mail: d.elhamifar@yu.ac.ir

as high thermal stability, adjustable hydrophobicity, low vapor pressure, and high conductivity make ILs an excellent stabilizer for TMs.[48]

According to the above, in this research work, a novel ionic liquid-modified magnetic graphene oxide nanocomposite supported palladium (Fe_3O_4/GO–IL–Pd) catalyst has been prepared and characterized and its catalytic application has been investigated in the reduction of nitrobenzenes. The novelty of this work includes the use of non-toxic and green compounds such as ionic liquids and graphene oxide in the designed nanocomposite. The ionic liquid acts as a green medium that prevents the aggregation and leaching of palladium during the reaction process. Furthermore, graphene oxide, with its high surface area, enhances the loading of catalytically active sites. Additionally, Fe_3O_4 imparts magnetic properties to the catalyst, allowing for easy separation and recovery using an external magnetic field. These features result in low toxicity, good biocompatibility, high catalytic activity, and high recoverability of the designed composite.

2. Experimental section

2.1. General

All chemicals including iron(II) chloride tetrahydrate (99%), iron(III) chloride hexahydrate (99%), tetramethoxysilane (TMOS, 99%), (3-aminopropyl)triethoxysilane (APTES, 98%), graphite powder, benzaldehydes (97–99%), palladium acetate (98%), DMSO, toluene and ethanol were purchased from Fluka, Merck and Sigma-Aldrich companies. Energy-dispersive X-ray spectroscopy (EDS) was performed using a SAMX (France) EDS instrument. The morphology of the particles was determined by using a SIGMA VP scanning electron microscope (FE-SEM) (Germany). Fourier transform infrared (FT-IR) spectroscopy was performed on a Bruker-Vector 22 spectrometer (Germany). Powder X-ray diffraction (PXRD) was performed using a Bruker D8 ADVANCE diffractometer (Germany). Thermal gravimetric analysis (TGA) was carried out using a Netzsch STA 409 PC/PG apparatus (Germany). The magnetic properties were measured by using a vibrating sample magnetometer (VSM) of Meghnatis Daghigh Kavir Company (Iran).

2.2. Preparation of Fe_3O_4@SiO_2–NH/GO

At first, 0.5 g of graphene oxide was well dispersed in 20 mL of water for 20 minutes. Then, 1 g of Fe_3O_4@SiO_2[49] was added to the reaction vessel. The obtained mixture was heated to 70 °C and 0.5 mL of (3-aminopropyl)triethoxysilane (APTES) was added drop by drop while stirring vigorously for 3 hours. The product was magnetically separated and after washing with ethanol, it was dried at 65 °C for 7 h and denoted as Fe_3O_4@SiO_2–NH/GO.

2.3. Preparation of Fe_3O_4@SiO_2–NH/GO–IL

For this, first, 1 g of Fe_3O_4@SiO_2–NH/GO nanocomposite was well dispersed in 50 mL of toluene. Then, 0.5 mmol of 1-methyl-3-(3-trimethoxysilylpropyl)imidazolium chloride was added and the obtained mixture was refluxed for 24 hours in an oil bath. The resulting material was separated using an external magnet, washed with ethanol, dried at 65 °C for 6 h, and denoted as Fe_3O_4@SiO_2–NH/GO–IL.

2.4. Preparation of Fe_3O_4@SiO_2–NH/GO–IL–Pd

For this, 1 g of Fe_3O_4@SiO_2–NH/GO–IL was completely dispersed in 30 mL of DMSO. After adding 1.5 mmol of $Pd(OAc)_2$, the obtained combination was stirred at RT for 24 h. The resulting material was separated by using an external magnet, washed with ethanol and distilled water, dried at 65 °C for 6 h, and denoted as Fe_3O_4/GO–IL–Pd. According to the ICP analysis, the loading of palladium in/on the material framework was found to be 0.29 mmol Pd per one gram of Fe_3O_4/GO–IL–Pd.

2.5. Reduction of nitrobenzenes using Fe_3O_4/GO–IL–Pd

For this, 1 mmol of nitrobenzene derivative, 0.05 g of the Fe_3O_4/GO–IL–Pd catalyst (1.45 mol% pd), and 5 mL of water were well mixed at RT. After adding 2 mmol of $NaBH_4$, the obtained combination was stirred at RT for the appropriate time indicated in Table 2. Upon the completion of the reaction, Fe_3O_4/GO–IL–Pd was separated by using an external magnet, and aniline derivatives resulted after the recrystallization of the crude mixture in EtOH.

3. Results and discussion

The preparation of the Fe_3O_4/GO–IL–Pd nanocomposite is shown in Scheme 1. First, graphene oxide was reacted with propylamine-modified Fe_3O_4@SiO_2 (Fe_3O_4@SiO_2–NH_2) to deliver the Fe_3O_4@SiO_2–NH_2/GO nanocomposite. Then, the surface of Fe_3O_4@SiO_2–NH_2/GO was chemically modified with IL to give the Fe_3O_4@SiO_2–NH_2/GO–IL material. Finally, this material was treated with palladium acetate salt to deliver the Fe_3O_4/GO–IL–Pd nanocatalyst. The PXRD, FT-IR, SEM, EDS, EDS-mapping, and TG analyses were used to characterize this catalyst.

The FT-IR analysis of GO and Fe_3O_4/GO–IL–Pd is shown in Fig. 1. For these samples, the strong peak at 3474 cm^{-1} is due to the O–H bonds of the material surface. For Fe_3O_4/GO–IL–Pd, the signals at 2835 and 2945 cm^{-1} are attributed to the C–H bonds of IL-propyl groups (Fig. 1b). Also, the peaks at 1750, 1625, and 1100 cm^{-1} are related to carboxyl C=O, aromatic C=C, and C–O bonds of GO, respectively (Fig. 1a and b).[50] Moreover, the peaks at 110 and 550 cm^{-1} are corresponded to the Si–O–Si and Fe–O bonds of Fe_3O_4/GO–IL–Pd, respectively (Fig. 1b).[51]

The scanning electron microscopy (SEM) analysis was performed to study the morphology of the Fe_3O_4@SiO_2 and Fe_3O_4/GO–IL–Pd materials (Fig. 2). As shown, the Fe_3O_4@SiO_2 nanoparticles exhibit a predominantly spherical morphology (Fig. 2a). The SEM image of Fe_3O_4/GO–IL–Pd clearly showed that the Fe_3O_4@SiO_2 NPs are uniformly dispersed across the layered and folded surface of the GO (Fig. 2b), indicating the successful stabilization of Fe_3O_4@SiO_2 NPs to GO.

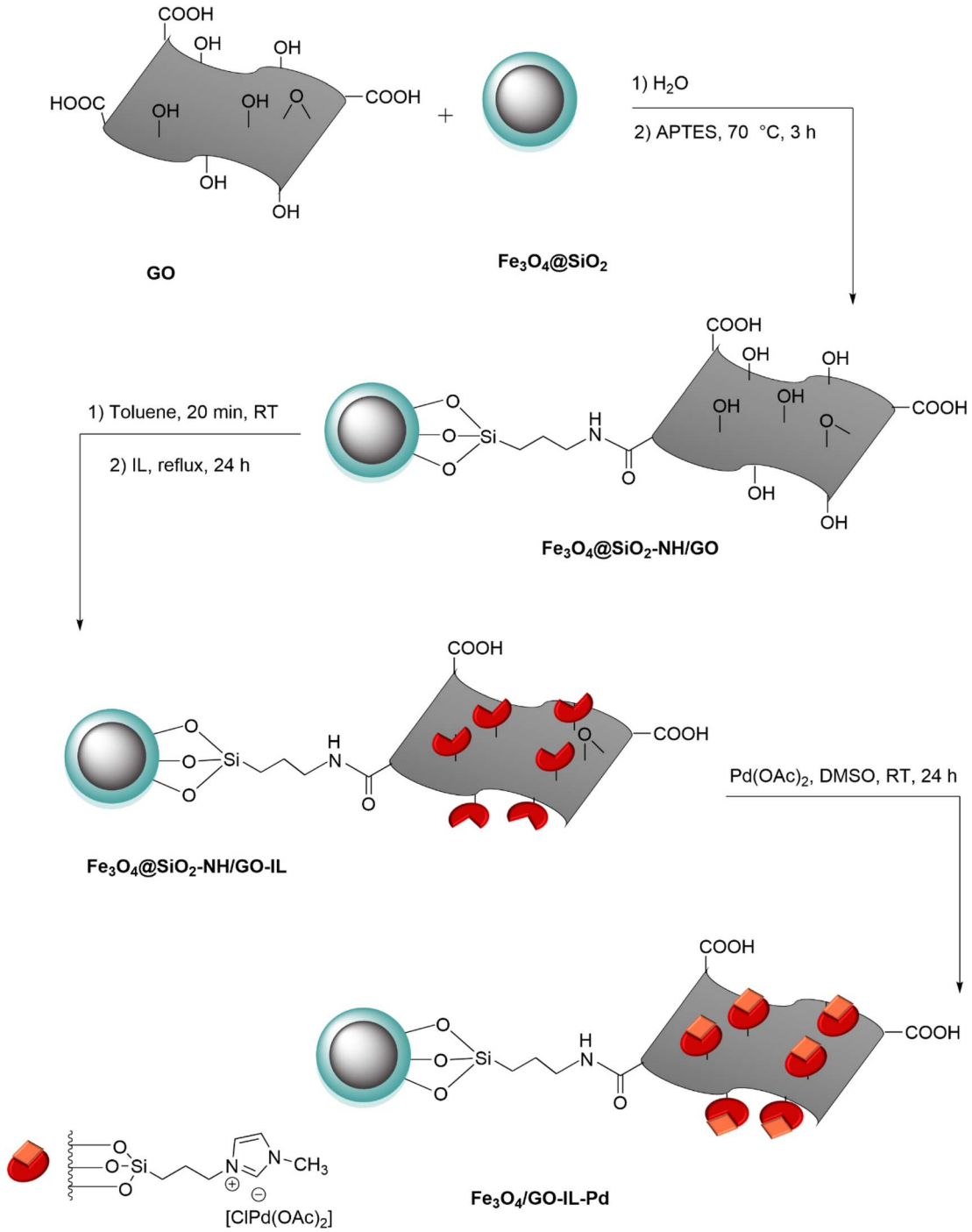

Scheme 1 Preparation of Fe_3O_4/GO–IL–Pd.

EDS analysis of the Fe_3O_4/GO–IL–Pd nanocatalyst showed the existence of N, O, C, Si, Fe, and Pd signals (Fig. 3). This confirms the successful immobilization of the ionic liquid/Pd complex on Fe_3O_4/GO.

The EDS mapping analysis also showed that all the above-mentioned elements are well distributed in the prepared nanocomposite (Fig. 4).

The magnetic characteristics of the prepared nanocomposites were considered using VSM analysis. It was found that the saturation magnetization values of Fe_3O_4, Fe_3O_4@SiO_2, and Fe_3O_4/GO–IL–Pd magnetic nanocomposites are, respectively, 66, 55, and 40 emu g^{-1}. The reduction in magnetic properties after the modification process confirms the successful coating of silica and functionalized graphene oxide on the surface of the Fe_3O_4

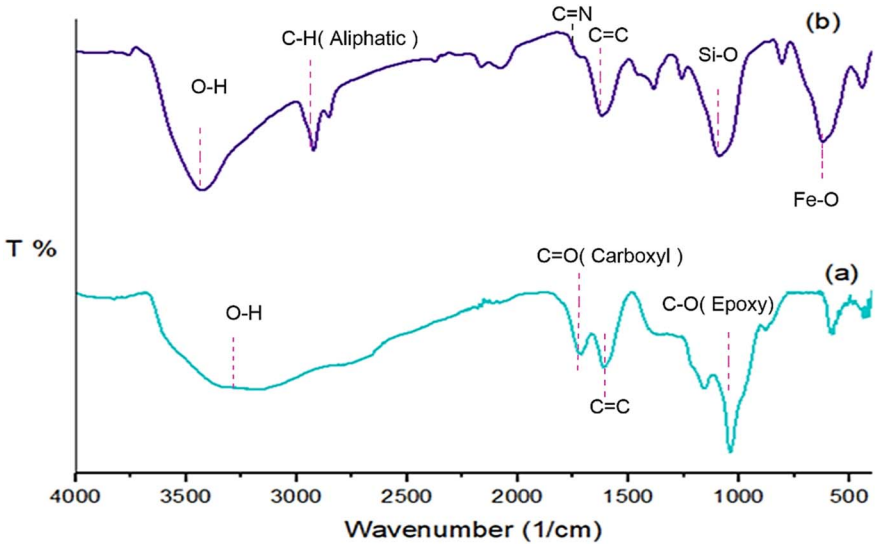

Fig. 1 FT-IR of (a) GO and (b) Fe_3O_4/GO–IL–Pd.

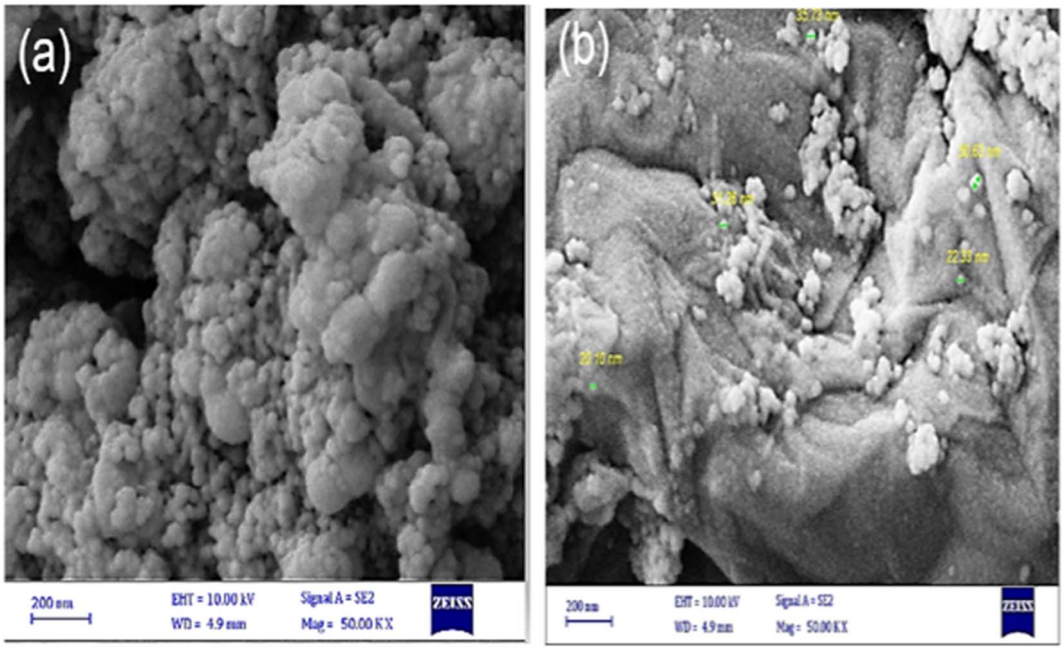

Fig. 2 SEM image of (a) Fe_3O_4@SiO_2 and (b) Fe_3O_4/GO–IL–Pd.

nanoparticles (Fig. 5). This characteristic is very important, especially in the catalysis and adsorption processes.

The thermal stability of the designed Fe_3O_4/GO–IL–Pd nanocomposite was investigated by TG analysis (Fig. 6). The TGA results showed three weight losses at 10–150 °C, 151–230 °C and 235–560 °C. The first weight loss (10 to 150 °C) is related to the solvent removal from the surface of the nanocomposite. The second weight loss in the range of 151 to 230 °C is attributed to the elimination of the immobilized organic groups (ionic liquid and propyl amine) from the nanocomposite structure. The final weight loss at temperatures above 235 °C is assigned to the removal of remaining ionic liquids and also the decomposition of GO moieties.

The crystalline structures of the Fe_3O_4, Fe_3O_4@SiO_2–NH/GO, and Fe_3O_4/GO–IL–Pd nanomaterials were evaluated by powder XRD analysis (Fig. 7). As seen, the PXRD pattern of all materials demonstrates eight characteristic peaks at 2θ of 18.3°, 30.3°, 35.6°, 43.3°, 53.7°, 57.4°, 63°, and 74.3° corresponding, respectively, to the (111), (220), (311), (400), (422), (511), (440) and (533) planes. The pattern is completely matched with that

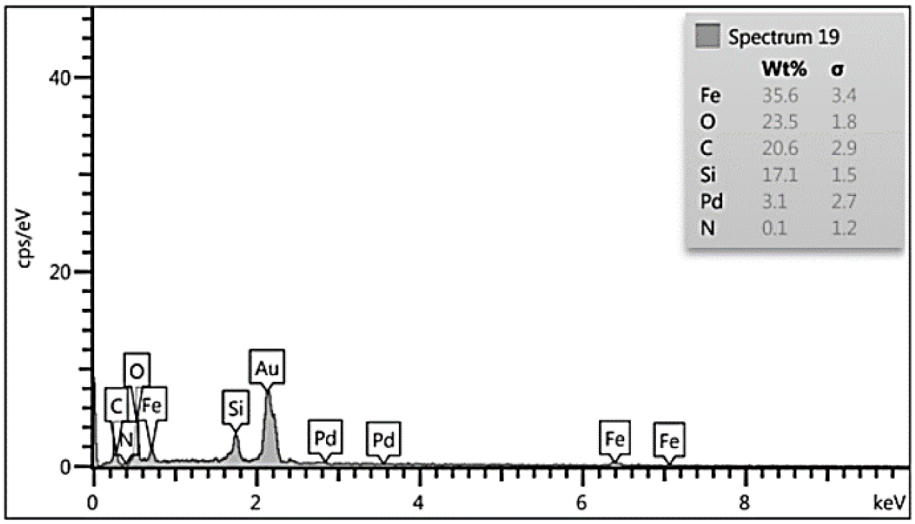

Fig. 3 EDS analysis of Fe_3O_4/GO–IL–Pd.

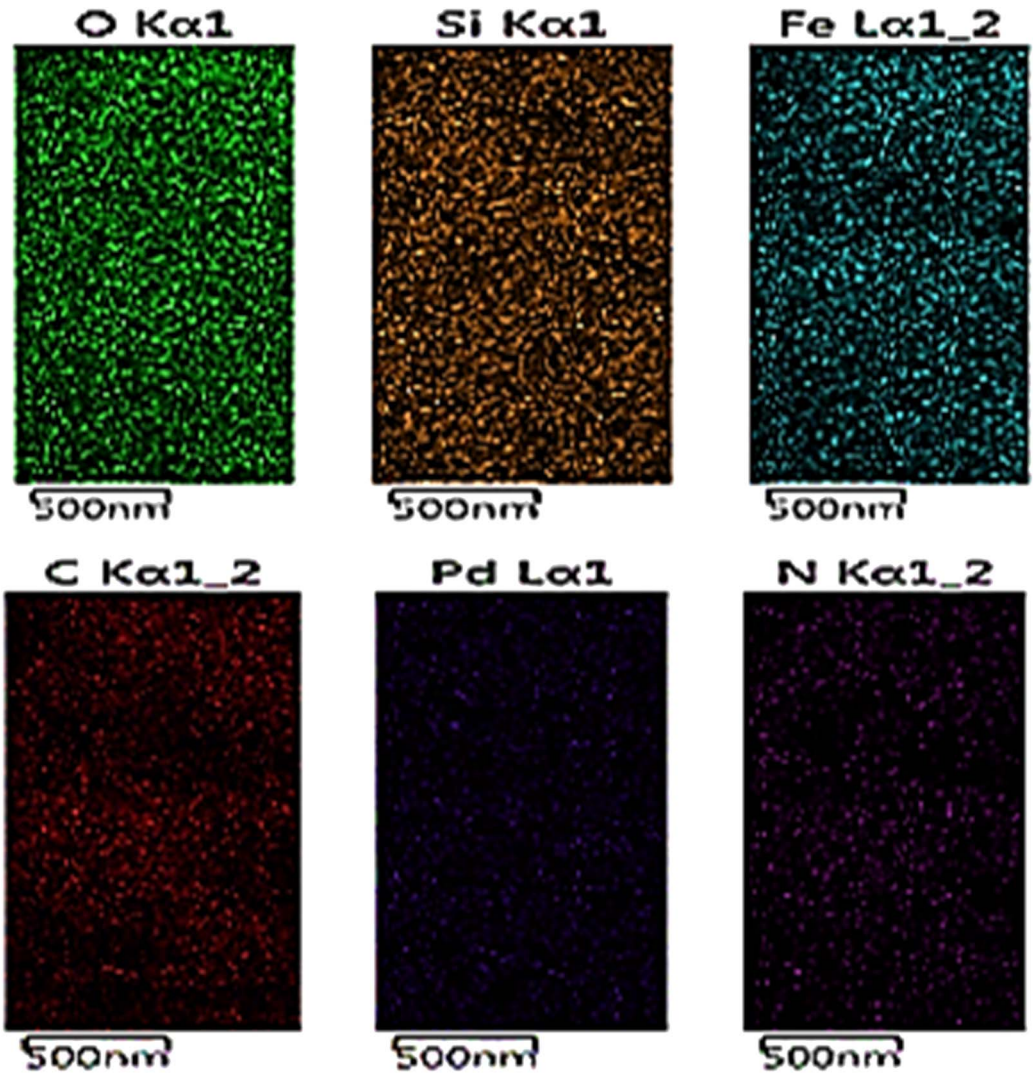

Fig. 4 EDS mapping of Fe_3O_4/GO–IL–Pd.

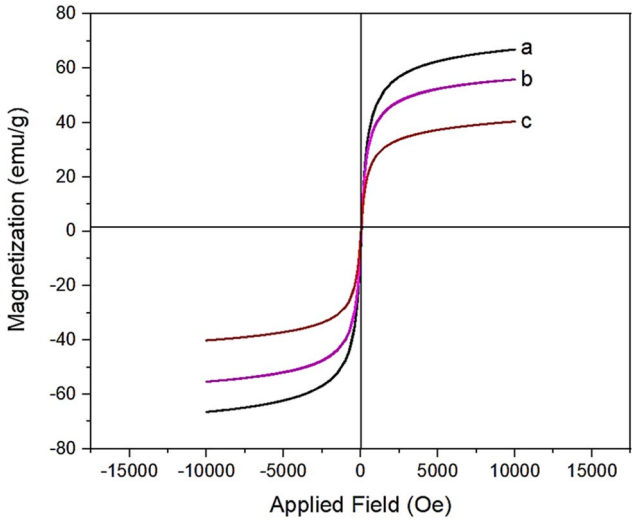

Fig. 5 VSM diagrams of (a) Fe_3O_4, (b) Fe_3O_4@SiO_2 and (c) Fe_3O_4/GO–IL–Pd.

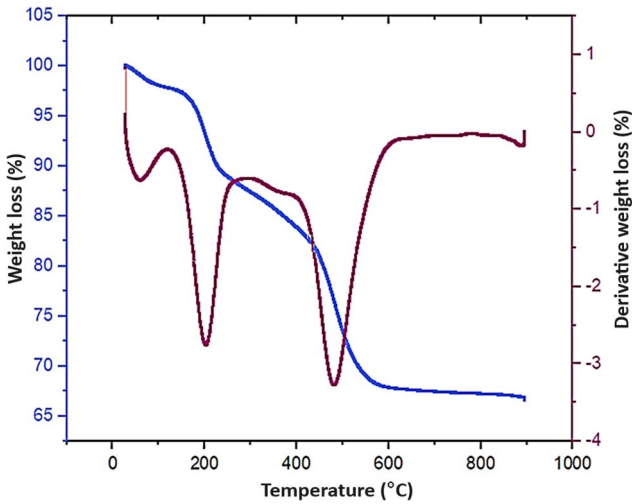

Fig. 6 TGA of Fe_3O_4/GO–IL–Pd.

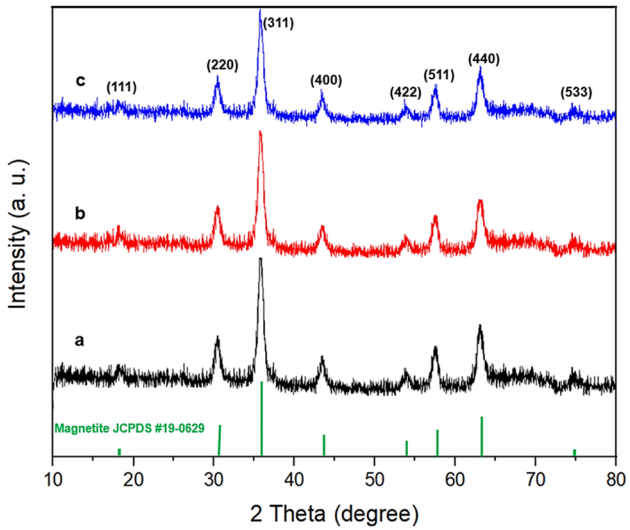

Fig. 7 PXRD pattern of (a) Fe_3O_4, (b) Fe_3O_4@SiO_2–NH/GO and (c) Fe_3O_4/GO–IL–Pd.

Table 1 Optimization of the reaction conditions in the reduction of nitrobenzene

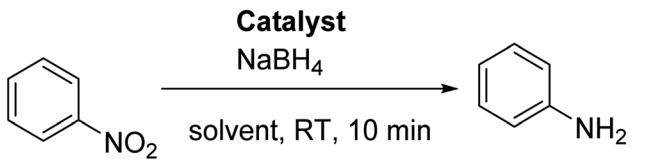

Entry	Catalyst (g)	Solvent	TON[a]	TOF[b]	Yield (%)
1	Fe_3O_4/GO–IL–Pd (0.03)	EtOH	59.8	373.75	52
2	Fe_3O_4/GO–IL–Pd (0.03)	MeOH	55.17	344.81	48
3	Fe_3O_4/GO–IL–Pd (0.03)	Water	80.45	281.25	70
4	Fe_3O_4/GO–IL–Pd (0.05)	Water	65.51	409.43	95
5	Fe_3O_4/GO–IL–Pd (0.08)	Water	40.94	255.87	95
6	Fe_3O_4/GO–IL (0.05)	Water	—	—	N. R.
7	Fe_3O_4/GO (0.05)	Water	—	—	N. R.
8	Fe_3O_4@SiO_2–NH_2 (0.05)	Water	—	—	N. R.

[a] Turnover number [defined as yield (%)/cat. (mol%)]. [b] Turnover frequency [defined as TON/reaction time (h)].

of the Fe_3O_4 standard sample (JCPDS card, file no. 19-0629).[52–54] This finding indicates that the Fe_3O_4 NPs have preserved their crystalline structure during the modification steps.[55,56]

After characterization, the prepared Fe_3O_4/GO–IL–Pd nanocatalyst was used in the reduction of nitrobenzenes at RT. Optimal conditions were determined by examining the impact of the nanocatalyst and solvents (water, ethanol, and methanol) on the reduction of nitrobenzene in the presence of $NaBH_4$ as a model reaction (Table 1). It was found that switching the solvent from ethanol and methanol to water improves catalytic efficiency and reaction yield (Table 1, entries 1–3). The study also demonstrated that in the presence of 0.05 g of Fe_3O_4/GO–IL–Pd nanocatalyst (1.45 mol% Pd), the best yield is obtained (Table 1, entries 3–5). Importantly, where the reaction was done using Pd-free Fe_3O_4/GO–IL, Fe_3O_4@SiO_2–NH/GO, and Fe_3O_4@SiO_2–NH_2 nanocomposites (Table 1, entries 6–8), no product was obtained, confirming that the reaction is catalyzed by immobilized palladium species. Accordingly, the use of 0.05 g of Fe_3O_4/GO–IL–Pd, water solvent, and RT were selected as optimum conditions (Table 1, entry 4).

After optimization of the conditions, different nitrobenzenes were used as substrates to check the activity of the catalyst. The results showed that all nitrobenzene derivatives containing both electron-donating and electron-withdrawing substituents deliver corresponding aniline products in a high yield. This finding confirms the high performance of the designed Fe_3O_4/GO–IL–Pd catalyst in the reduction of a wide range of

Table 2 Reduction of nitrobenzene derivatives in the presence of the Fe_3O_4/GO–IL–Pd nanocomposite[a]

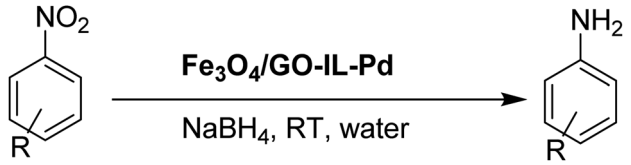

Entry	R	Time (min)	Yield (%)	TON	TOF	Mp (°C) found	Mp (°C) reported
1	H	10	95	65.51	409.43	181–183	182–184 [ref. 57]
2	4-NH_2	15	95	65.51	262.04	138–140	136–139 [ref. 58]
3	2-OH	10	89	61.37	383.56	171–173	170–75 [ref. 51]
4	4-OH	10	96	66.20	413.75	182–184	181–183 [ref. 58]
5	3-CHO	15	95	65.51	262.04	91–93	92–95 [ref. 59]

[a] Reaction conditions: nitrobenzene (1 mmol), $NaBH_4$ (2 mmol), Fe_3O_4/GO–IL–Pd catalyst (0.05 g containing 1.45 mol% Pd), H_2O (5 mL) and RT.

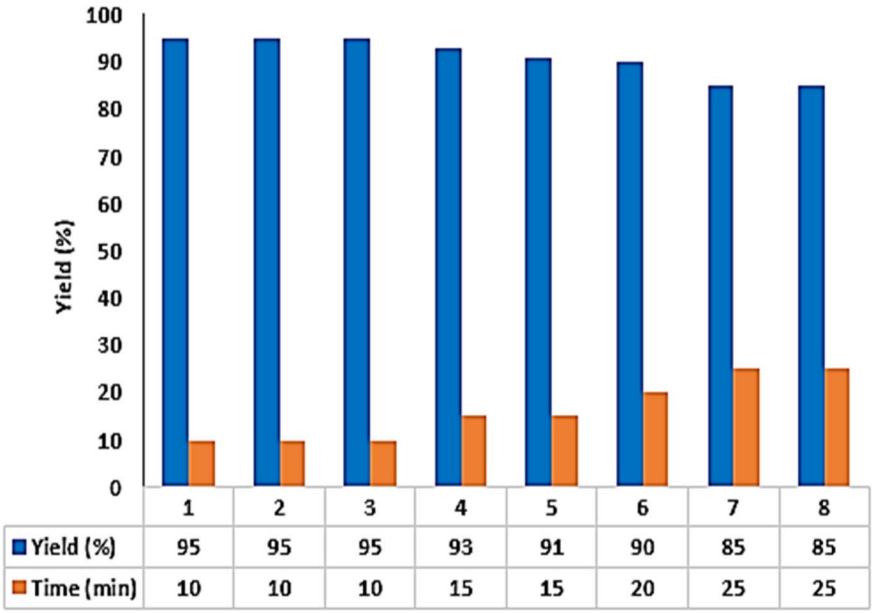

Fig. 8 Recoverability and reusability of the Fe_3O_4/GO–IL–Pd catalyst.

nitrobenzenes (Table 2). It is important to note that where 3-nitrobenzaldehyde was used as a substrate, 2 mol% of catalyst and 3 mmol of $NaBH_4$ were used. In this reaction, both nitro and aldehyde substituents were reduced, respectively, to corresponding amine and alcohol groups (Table 2, entry 5).

Next, the recoverability and reusability of Fe_3O_4/GO–IL–Pd were tested in the model reaction. To do this, after the reaction was completed, the catalyst was separated by using a magnet, washed with ethanol, dried, recovered, and reused in the next run. These steps were repeated several times and it was found that the Fe_3O_4/GO–IL–Pd catalyst could be reused at least seven times while maintaining its performance (Fig. 8).

A leaching experiment was also done to investigate the nature of Fe_3O_4/GO–IL–Pd under applied conditions. To do this, after 45% progress of the reaction, Fe_3O_4/GO–IL–Pd was separated using a magnet. Then, the reaction development of the residue was checked for 2 h, in which no significant yield was seen. The analysis of atomic absorption (AA) also showed no presence of palladium in the residue confirming high stability and no leaching of supported Pd species under applied conditions.

To investigate the chemical and structural stability of the catalyst under the applied conditions, PXRD, SEM, and EDS analyses were conducted on the recovered catalyst after seven recovery times. As illustrated in Fig. 9, the PXRD pattern of the recovered Fe_3O_4/GO–IL–Pd catalyst exhibited eight peaks at $2\theta = 18.3°$, 30.3°, 35.6°, 43.3°, 53.7°, 57.4°, 63°, and 74.3° which is in good agreement with the PXRD pattern of the fresh

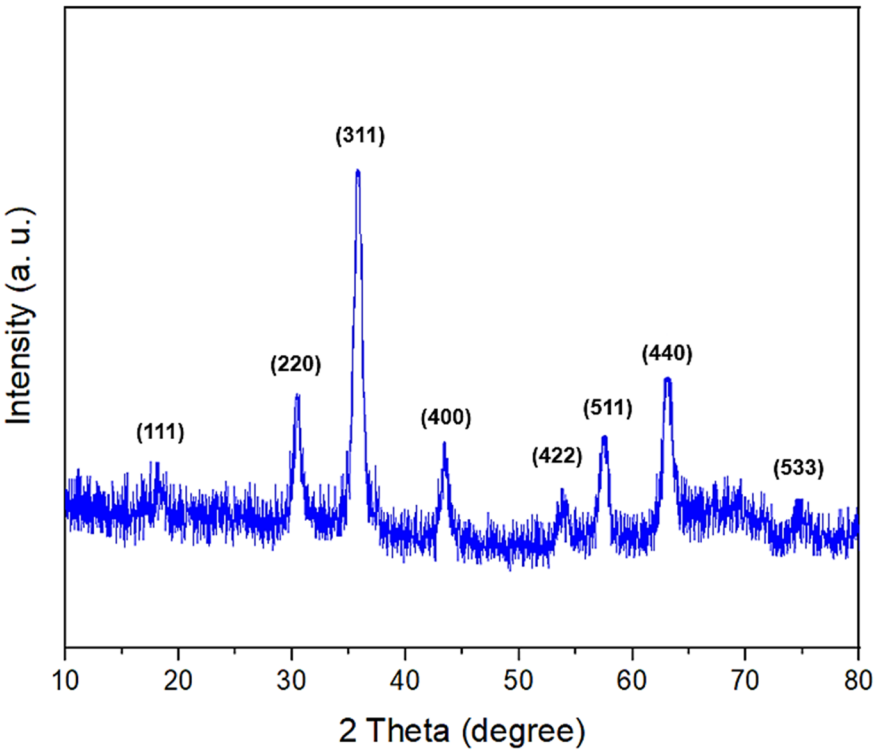

Fig. 9 PXRD pattern of the recovered Fe_3O_4/GO–IL–Pd catalyst.

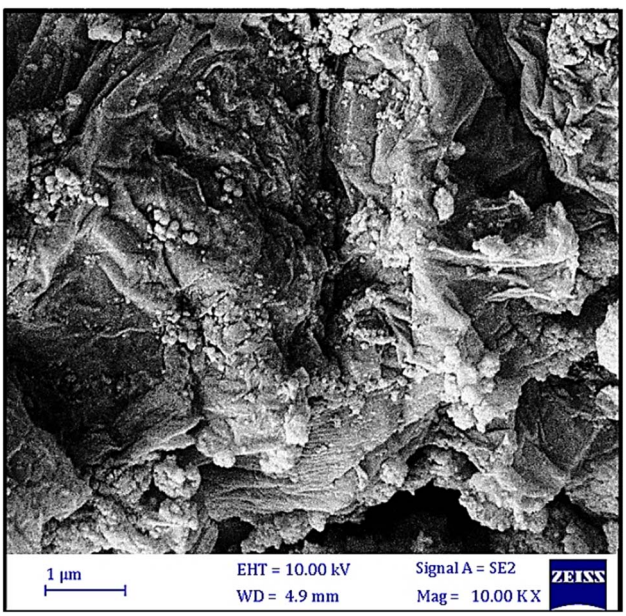

Fig. 10 SEM image of the recovered Fe_3O_4/GO–IL–Pd catalyst.

nanocatalyst. This analysis confirms the remarkable stability of the crystalline structure of magnetite NPs after multiple cycles of reuse and recovery.

The SEM image of the recovered Fe_3O_4/GO–IL–Pd catalyst also revealed a morphology similar to that of the fresh catalyst, confirming the high structural stability of the designed material under the applied conditions (Fig. 10).

As depicted in Fig. 11, the EDS pattern of the recovered catalyst exhibits no significant difference compared to the EDS of the fresh Fe_3O_4/GO–IL–Pd catalyst. These findings demonstrate the high stability of the catalyst following multiple cycles of recovery and reuse.

A plausible mechanism for the reduction of nitrobenzenes using the Fe_3O_4/GO–IL–Pd catalyst is presented in Scheme 2. In this mechanism, borohydride ions (BH_4^-) are dispersed and adsorbed onto the nanocomposite surface, facilitating electron transfer from $NaBH_4$ to the nitroarene compound, mediated by palladium. The nucleophilic attack of negatively charged hydrogen at the Pd–H site on the electrophilic nitro functional group, followed by hydrogen transfer, leads to the formation of the reduced product.[60]

Finally, the performance of the designed Fe_3O_4/GO–IL–Pd catalyst was compared with that of the reported catalysts in the model reaction (Table 3). As shown, the designed nanocomposite is relatively more efficient than the previous catalysts, especially in terms of recovery times and solvent usage. The higher performance of Fe_3O_4/GO–IL–Pd may be attributed to its magnetic nature, as well as the key role of immobilized ILs in protecting Pd species from leaching.

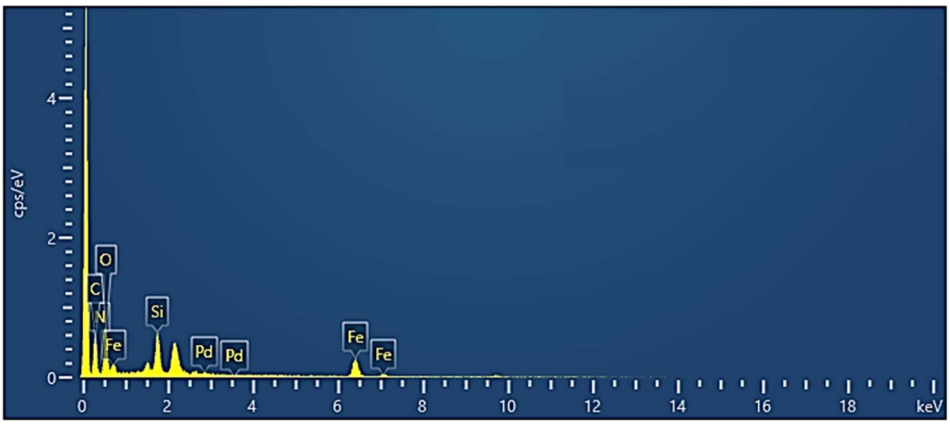

Fig. 11 EDS spectrum of the recovered Fe_3O_4/GO–IL–Pd catalyst.

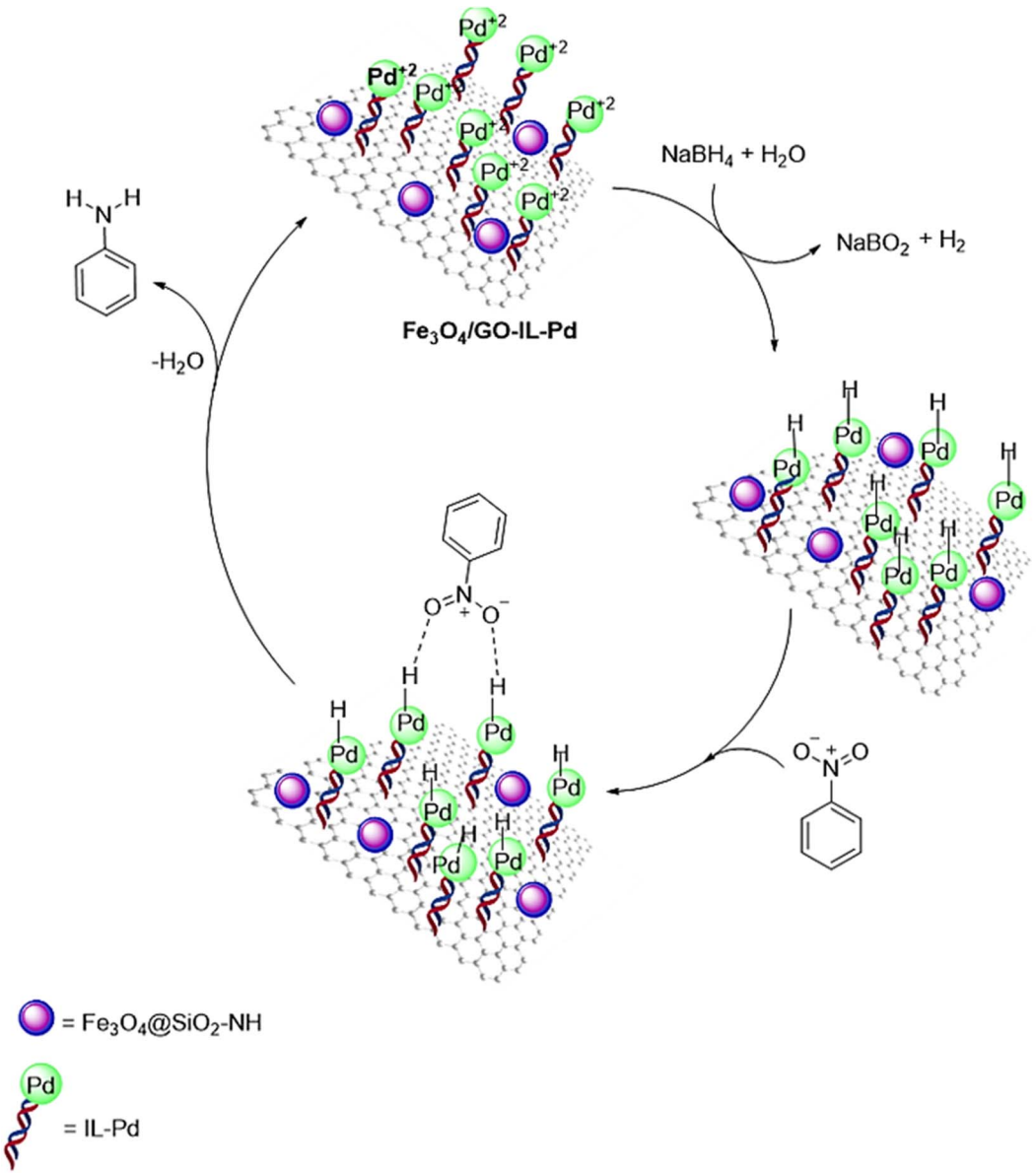

Scheme 2 A plausible mechanism for the reduction of nitrobenzenes using Fe_3O_4/GO–IL–Pd.

Table 3 Comparison of the catalytic performance of Fe_3O_4/GO–IL–Pd with that of previously reported catalysts in the reduction of nitrobenzene

Catalyst	Conditions	Yield (%)	Recovery times	Ref.
NiNPs/DNA	H_2O, $NaBH_4$, RT, 2 h, 2 mol% of catalyst	99	4	61
CuO–GO	H_2O, $NaBH_4$, RT, 30 min, 50 mg of catalyst	98	5	62
Fe_3O_4@Cur/Mel-Ag	$NaBH_4$ (2.0 mmol)/0.04 g K_2CO_3/pH (8.0), 70 °C, 10 min, 0.02 g of catalyst	98	4	63
GA–Pd/ZnO	MeOH, H_2 atmosphere, RT, 2 h, 10 mg of catalyst	98	4	64
Fe_3O_4/GO–IL–Pd	Water, $NaBH_4$, RT, 10 min, 0.05 g of catalyst	95	7	This work

4. Conclusion

In this work, a magnetic nanocomposite containing Fe_3O_4@-SiO_2 and graphene oxide (GO) modified with an ionic liquid–Pd complex (Fe_3O_4/GO–IL–Pd) was prepared, characterized, and applied as a powerful catalyst for the reduction of nitrobenzenes. The SEM image showed a morphology containing layered graphene oxide and spherical iron oxide nanoparticles. The EDS analysis confirmed the good distribution of expected C, N, O, Si, Pd, and Fe elements in the designed nanocomposite. The good magnetic properties of the Fe_3O_4/GO–IL–Pd nanocomposite were confirmed by using VSM analysis. The TG analysis showed high thermal stability of the synthesized nanocomposite. The FT-IR analysis confirmed the successful synthesis of the expected functional groups in this nanocomposite.[65] The PXRD pattern also confirmed that the crystallinity of Fe_3O_4 NPs is preserved after modification steps.[66–68] The Fe_3O_4/GO–IL–Pd nanocomposite was successfully used as a catalyst in the reduction of nitrobenzenes giving corresponding anilines in high yield. The Fe_3O_4/GO–IL–Pd nanocatalyst was recovered and reused seven times with no significant decrease in its performance. The high durability and stability of the recovered catalyst were confirmed by using PXRD, SEM, and EDS analyses.

Data availability

The original contributions presented in the study are included in the article, further inquiries can be directed to the corresponding author.

Conflicts of interest

There are no conflicts to declare.

Acknowledgements

The authors thank Yasouj University and the Iran National Science Foundation (INSF) for supporting this work.

References

1 L. Wang, P. Li, Z. Wu, J. Yan, M. Wang and Y. Ding, *Synthesis*, 2003, **2003**, 2001–2004.
2 S. Piña Jr, D. M. Cedillo, C. Tamez, N. Izquierdo, J. G. Parsons and J. J. Gutierrez, *Tetrahedron Lett.*, 2014, **55**, 5468–5470.
3 N. Daems, J. Wouters, C. Van Goethem, K. Baert, C. Poleunis, A. Delcorte, A. Hubin, I. F. Vankelecom and P. P. Pescarmona, *Appl. Catal., B*, 2018, **226**, 509–522.
4 F. Harraz, S. El-Hout, H. Killa and I. Ibrahim, *J. Catal.*, 2012, **286**, 184–192.
5 J. Wang, Z. Yuan, R. Nie, Z. Hou and X. Zheng, *Ind. Eng. Chem. Res.*, 2010, **49**, 4664–4669.
6 P. Lara and K. Philippot, *Catal. Sci. Technol.*, 2014, **4**, 2445–2465.
7 A. Corma, C. González-Arellano, M. Iglesias and F. Sánchez, *Appl. Catal.*, 2009, **356**, 99–102.
8 S. Menuel, B. Léger, A. Addad, E. Monflier and F. Hapiot, *Green Chem.*, 2016, **18**, 5500–5509.
9 C. T. Redemann and C. E. Redemann, *Org. Synth.*, 2003, **29**, 8.
10 K. Abiraj, G. R. Srinivasa and D. C. Gowda, *Can. J. Chem.*, 2005, **83**, 517–520.
11 J. Kielhorn, C. Melber, D. Keller and I. Mangelsdorf, *Int. J. Hyg. Environ. Health*, 2002, **205**, 417–432.
12 L. L. Jewell and B. H. Davis, *Appl. Catal.*, 2006, **310**, 1–15.
13 X.-F. Wu, H. Neumann and M. Beller, *Chem. Rev.*, 2013, **113**, 1–35.
14 M. Khanmohammadi, S. Amani, A. B. Garmarudi and A. Niaei, *Chin. J. Catal.*, 2016, **37**, 325–339.
15 J. C. Védrine, *Chin. J. Catal.*, 2019, **40**, 1627–1636.
16 J. Tang, S. Zhang, X. Chen, L. Zhang, L. Du and Q. Zhao, *Catalysts*, 2023, **13**, 956.
17 H. Veisi, B. Karmakar, T. Tamoradi, R. Tayebee, S. Sajjadifar, S. Lotfi, B. Maleki and S. Hemmati, *Sci. Rep.*, 2021, **11**, 4515.
18 X. Lu, J. He, R. Jing, P. Tao, R. Nie, D. Zhou and Q. Xia, *Sci. Rep.*, 2017, **7**, 2676.
19 T. Windhorst and G. Blount, *Mater. Des.*, 1997, **18**, 11–15.
20 C. Hu, Y. Lin, J. W. Connell, H. M. C. heng, Y. Gogotsi, M. Titirici and L. Dai, *Adv. Mater.*, 2019, **31**(13), 1806128.
21 F. Dénès, A. Pérez-Luna and F. Chemla, *Chem. Rev.*, 2010, **110**, 2366–2447.
22 M. Azizi-Lalabadi, H. Hashemi, J. Feng and S. M. Jafari, *Adv. Colloid Interface Sci.*, 2020, **284**, 102250.
23 M. J. Sweetman, S. May, N. Mebberson, P. Pendleton, K. Vasilev, S. E. Plush and J. D. Hayball, *C*, 2017, **3**, 18.
24 A. B. Seabra, A. J. Paula, R. de Lima, O. L. Alves and N. Durán, *Chem. Res. Toxicol.*, 2014, **27**, 159–168.
25 W. Yu, L. Sisi, Y. Haiyan and L. Jie, *RSC Adv.*, 2020, **10**, 15328–15345.

26 D. C. Marcano, D. V. Kosynkin, J. M. Berlin, A. Sinitskii, Z. Sun, A. Slesarev, L. B. Alemany, W. Lu and J. M. Tour, *ACS Nano*, 2010, **4**, 4806–4814.
27 C. Chung, Y.-K. Kim, D. Shin, S.-R. Ryoo, B. H. Hong and D.-H. Min, *Acc. Chem. Res.*, 2013, **46**, 2211–2224.
28 M. F. Lanjwani, M. Tuzen, M. Y. Khuhawar and T. A. Saleh, *Inorg. Chem. Commun.*, 2024, **159**, 111613.
29 R. Ullah and M. Tuzen, *J. Mol. Struct.*, 2023, **1285**, 135509.
30 J. Ali, S. Bibi, W. B. Jatoi, M. Tuzen, M. A. Jakhrani, X. Feng and T. A. Saleh, *Mater. Today Commun.*, 2023, 106840.
31 Z. Ali, R. Ullah, M. Tuzen, S. Ullah, A. Rahim and T. A. Saleh, *Trends Environ. Anal. Chem.*, 2023, **37**, e00187.
32 M. Amiri, H. Salehniya and A. Habibi-Yangjeh, *Ind. Eng. Chem. Res.*, 2016, **55**, 8114–8122.
33 Z. Cheng, Y. Dai, X. Kang, C. Li, S. Huang, H. Lian, Z. Hou, P. Ma and J. Lin, *Biomaterials*, 2014, **35**, 6359–6368.
34 M. Dolatabadi, T. Świergosz, C. Wang and S. Ahmadzadeh, *Arabian J. Chem.*, 2023, **16**, 104424.
35 A. H. Cahyana, A. R. Liandi, M. Maghdalena, R. T. Yunarti and T. P. Wendari, *Ceram. Int.*, 2022, **48**, 18316–18323.
36 N. Chadha, M. Y. Bhat, S. Hashmi and P. Saini, *J. Energy Storage*, 2022, **46**, 103789.
37 A. H. Mahvi, D. Balarak and E. Bazrafshan, *Int. J. Environ. Anal. Chem.*, 2023, **103**, 3501–3521.
38 M.-L. Ye, Y. Zhu, Y. Lu, L. Gan, Y. Zhang and Y.-G. Zhao, *Talanta*, 2021, **230**, 122299.
39 A. Kirschning, L. Kupracz and J. Hartwig, *Chem. Lett.*, 2012, **41**, 562–570.
40 L. Nirumand and S. Farhadi, *New J. Chem.*, 2023, **47**, 4845–4859.
41 M. Yan, Q. Liang, W. Wan, Q. Han, S. Tan and M. Ding, *RSC Adv.*, 2017, **7**, 30109–30117.
42 Y. Li, J. Qiu, S. Ye, L. Wang, C. Yang, P. Sun and C. Wang, *New J. Chem.*, 2017, **41**, 14137–14144.
43 Y. Zhu, S. Cheng, W. Zhou, J. Jia, L. Yang, M. Yao, M. Wang, J. Zhou, P. Wu and M. Liu, *ACS Sustain. Chem. Eng.*, 2017, **5**, 5067–5074.
44 P. Hariani, M. Said, R. A. Salni, N. Aprianti and E. Sthephanie, *Global NEST J.*, 2023, **25**, 36–43.
45 H. Zhang, X. Tian, C. Wang, H. Luo, J. Hu, Y. Shen and A. Xie, *Appl. Surf. Sci.*, 2014, **314**, 228–232.
46 M. Neysi and D. Elhamifar, *Front. Chem.*, 2023, **11**, 1112911.
47 N. V. Plechkova and K. R. Seddon, *Chem. Soc. Rev.*, 2008, **37**, 123–150.
48 B. Karimi, M. Tavakolian, F. Mansouri and H. Vali, *ACS Sustain. Chem. Eng.*, 2018, **7**, 3811–3823.
49 R. Nemati, D. Elhamifar, A. Zarnegaryan and M. Shaker, *Inorg. Chem. Commun.*, 2022, **145**, 109934.
50 U.-a. Kanta, V. Thongpool, W. Sangkhun, N. Wongyao and J. Wootthikanokkhan, *J. Nanomater.*, 2017, **2017**, 2758294.
51 P. Mofatehnia, G. M. Ziarani, D. Elhamifar and A. Badiei, *J. Phys. Chem. Solids*, 2021, **155**, 110097.
52 G. Antarnusa, P. D. Jayanti, Y. R. Denny and A. Suherman, *Materialia*, 2022, **25**, 101525.
53 E. Suharyadi, T. Alfansuri, L. S. Handriani, N. A. Wibowo and H. Sabarman, *J. Mater. Sci.: Mater. Electron.*, 2021, **32**, 23958–23967.
54 H. He, Y. Zhong, X. Liang, W. Tan, J. Zhu and C. Yan Wang, *Sci. Rep.*, 2015, **5**, 10139.
55 M. Vahidian, D. Elhamifar and M. Shaker, *Polyhedron*, 2020, **178**, 114326.
56 M. Shaker and D. Elhamifar, *Colloids Surf., A*, 2021, **608**, 125603.
57 A. C. Company, *Catalog Handbook of Fine Chemicals*, Aldrich Chemical Company, 2000.
58 Z. Kiani, R. Zhiani, S. Khosroyar, A. Motavalizadehkakhky and M. Hosseiny, *Inorg. Chem. Commun.*, 2021, **124**, 108382.
59 J. A. Lazzús, *Ind. Eng. Chem. Res.*, 2009, **48**, 8760–8766.
60 M. Gholinejad, M. Shojafar and J. M. Sansano, *J. Iran. Chem. Soc.*, 2020, **17**, 2033–2043.
61 M. Niakan and Z. Asadi, *Catal. Lett.*, 2019, **149**, 2234–2246.
62 K. Zhang, J. M. Suh, T. H. Lee, J. H. Cha, J. W. Choi, H. W. Jang, R. S. Varma and M. Shokouhimehr, *Nano Convergence*, 2019, **6**, 1–7.
63 N. Khaleghi, M. Forouzandeh-Malati, F. Ganjali, Z. Rashvandi, S. Zarei-Shokat, R. Taheri-Ledari and A. Maleki, *Sci. Rep.*, 2023, **13**(1), 5225.
64 P. Supriya, B. Srinivas, K. Chowdeswari, N. Naidu and B. Sreedhar, *Mater. Chem. Phys.*, 2018, **204**, 27–36.
65 K. Taheri, D. Elhamifar, S. Kargar and A. Zarnegaryan, *RSC Adv.*, 2023, **13**, 16067–16077.
66 M. Neysi and D. Elhamifar, *Front. Chem.*, 2024, **12**, 1336855.
67 R. Nemati, D. Elhamifar, A. Zarnegaryan and M. Shaker, *Appl. Organomet. Chem.*, 2021, **35**, e6409.
68 Z. Haydari, D. Elhamifar, M. Shaker and M. Norouzi, *Appl. Surf. Sci.*, 2021, **5**, 100096.